

Synthesis and characterization of ZnO and ZnO:Ga films and their application in dye-sensitized solar cells

Agnaldo de Souza Gonçalves,^{*a} Marian Rosaly Davolos,^a Naruhiko Masaki,^b Shozo Yanagida,^b Ana Morandeira,^c James R. Durrant,^c Jilian Nei Freitas^d and Ana Flávia Nogueira^{*d}

Received 31st October 2007, Accepted 4th January 2008

First published as an Advance Article on the web 12th February 2008

DOI: 10.1039/b716724e

Highly crystalline ZnO and Ga-modified zinc oxide (ZnO:Ga) nanoparticles containing 1, 3 and 5 atom% of Ga³⁺ were prepared by precipitation method at low temperature. The films were characterized by XRD, BET, XPS and SEM. No evidence of zinc gallate formation (ZnGa₂O₄), even in the samples containing 5 atom% of gallium, was detected by XRD. XPS data revealed that Ga is present into the ZnO matrix as Ga³⁺, according to the characteristic binding energies. The particle size decreased as the gallium level was increased as observed by SEM, which might be related to a faster hydrolysis reaction rate. The smaller particle size provided films with higher porosity and surface area, enabling a higher dye loading. When these films were applied to dye-sensitized solar cells (DSSCs) as photoelectrodes, the device based on ZnO:Ga 5 atom% presented an overall conversion efficiency of 6% (at 10 mW cm⁻²), a three-fold increase compared to the ZnO-based DSSCs under the same conditions. To our knowledge, this is one of the highest efficiencies reported so far for ZnO-based DSSCs. Transient absorption (TAS) study of the photoinduced dynamics of dye-sensitized ZnO:Ga films showed that the higher the gallium content, the higher the amount of dye cation formed, while no significant change on the recombination dynamics was observed. The study indicates that Ga-modification of nanocrystalline ZnO leads to an improvement of photocurrent and overall efficiency in the corresponding device.

Introduction

Great attention has been devoted to solar energy conversion by dye-sensitized solar cells (DSSCs) since the pioneering work reported by O'Regan and Grätzel,¹ especially in light of their low cost compared to conventional silicon solar cells. The device comprises a working electrode (usually a wide band gap semiconductor deposited in the form of a porous nanostructured film onto a transparent conductor oxide-TCO) sensitized by a ruthenium complex, usually the N3 or N-719 dye. This electrode is separated from the counter electrode (generally a Pt film deposited on a TCO) by an electrolyte (usually I₃⁻/I⁻ in a mixture of organic solvents). DSSCs based on TiO₂ as the nanostructured electrode are capable of achieving efficiencies of 11%.² Despite the fact that much work relies on DSSCs based on pure photoelectrodes, *i.e.*, not intentionally doped oxides such as TiO₂ and ZnO, some recent works have revealed high efficiencies obtained with nitrogen-doped titania electrode³ and (Al + W)-doped TiO₂.⁴ ZnO is a wide band gap semiconductor (~3.2 eV at room temperature) whose n-type behavior stems from its intrinsic oxygen deficiency (non-

stoichiometric oxide). Among their wide range of applications, ZnO films have potential to be applied as an alternative material for nanostructured electrodes in photoelectrochemical solar cells.⁵ The DSSCs based on ZnO have their solar conversion efficiencies limited, in part, by the formation of Zn²⁺/dye aggregates during the dye loading process depending on the dye composition, concentration and sensitization time.⁶ As reported earlier, the electron injection is decreased by the presence of aggregates on the surface of ZnO films.⁷ Besides, the molecules that are active for electron injection are attached directly to the ZnO surface while the aggregates are formed on this layer, according to the microscopic image of transient absorption.⁸ One reason for the improvement in the overall solar cell efficiency from 2 to 5% (AM 1.5, 10 mW cm⁻²) in DSSCs based on ZnO was the controlled dye-sensitization step through the addition of base to the dye solution or by shortening the sensitization time.⁶ Recently, the improvement of dye-loading in photoanodes came about by changing the microstructure of ZnO films⁵ yielding a conversion efficiency of 4.1% (AM 1.5, 100 mW cm⁻²) and 4.6% at low light power density (AM 1.5, 14 mW cm⁻²).

Although the strategy of doping the oxide semiconductors has generated promising results for TiO₂ films,^{3,4} the doping of ZnO with aluminium did not produce DSSCs with improved performance.^{9,10} Minami *et al.* have attempted to decrease the electric resistance of ZnO films by doping of group III elements such as B, Al, Ga and In.¹¹ Indeed, they reported an increase in carrier concentration after doping.¹¹ A myriad of applications such as transparent conductor oxide, laser diodes, *etc.* take advantage of the lower resistivity brought about by doping.¹² Nonaka *et al.*,

^aInstituto de Química, Universidade Estadual Paulista-UNESP, Araraquara, SP, Brazil

^bCenter for Advanced Science and Innovation, Osaka University, Suita, Osaka, 565-0871, Japan

^cCentre for Electronic Materials and Devices, Imperial College of Science Technology and Medicine, London, UK SW7 2AY

^dInstituto de Química, Universidade Estadual de Campinas-UNICAMP, Campinas, SP, Brazil. E-mail: anaflavia@iqm.unicamp.br; Fax: +55 19 3521 3023; Tel: +55 19 3521 3029

using molecular orbital calculations, demonstrated that new states originating from group III elements appear within the band gap.¹³

In this work we report DSSCs based on gallium-modified zinc oxide electrodes (ZnO:Ga) with improved efficiencies in comparison to pure ZnO based solar cells. In order to have more clear evidence of the gallium modification effect on the photovoltaic properties and on the film energetics, transient absorption spectroscopy (TAS) was used as a tool to probe the charge recombination dynamics in these films.

Experimental

ZnO and ZnO:Ga 1, 3 and 5 atom% nanoparticles were synthesized by adapting the procedure described in the literature.⁹ Zinc nitrate aqueous solution (0.1 mol L⁻¹ at pH 5) was mixed with 0.1 mol L⁻¹ triethanolamine. Gallium nitrate was used as the source of the Ga³⁺. The powder samples were characterized by X-ray diffractometry (XRD) using a Rigaku RINT 2000 (copper target, $\lambda = 1.5406 \text{ \AA}$). The colloidal solution was obtained by mixing ZnO or ZnO:Ga powder, deionized water, acetylacetone and Triton X-100. The resulting mixture was ground in a mortar for *ca.* 1 h. The paste was then applied on the conducting substrate (fluorine-doped SnO₂ glass, FTO) by the doctor blading technique. Adhesive tape (Scotch®) was used as frame and spacer. The semiconductor film was heated at 450 °C for 30 min to provide adequate electrical contact between the particles. The electrodes, while still warm (*ca.* 80 °C), were immersed into a 0.5 mmol L⁻¹ ethanolic solution of the complex [*cis*-bis(isothiocyanato)bis(2,2'-bipyridyl-4,4'-dicarboxylate)ruthenium(II) bis-tetrabutylammonium (also known as N-719, Solaronix) for 3 h at room temperature. Then, the sensitized films were rinsed with absolute ethanol to remove non-adsorbed N-719 species and allowed to dry in air. The liquid electrolyte was composed of 0.1 mol L⁻¹ LiI, 0.05 mol L⁻¹ I₂, 0.8 mol L⁻¹ tetrabutylammonium iodide, 0.5 mol L⁻¹ 4-*tert*-butylpyridine in 50% acetonitrile–50% 3-methoxypropionitrile. A Pt-sputtered FTO was used as the counter electrode. The cells were sealed by Himilan (Mitsui-Dupont Polychemicals). Film thickness was 6 μm (measured by the Sloan Technology profiler, Dektak 3) and the average cell area was 0.15 cm². The electrode morphology was observed by field emission scanning electron microscopy (SEM, Jeol JSM-6700FE). The X-ray photoelectron spectroscopy (XPS) was performed in a QuanterasXM PHI instrument using the Al-K α monochromatized X-ray source. The porosity and average pore size were estimated by the BET method based on nitrogen adsorption isotherm (Quantachrome, Autosorb 1) after scratching the films off the FTO. The pore size distribution estimated for the ZnO electrode was not clearly identified. Dye loading was determined according to a published procedure.⁵ The dye was desorbed from the porous film by using a 1 mol L⁻¹ NaOH solution (water–ethanol 1 : 1 volume ratio) and then analyzed in a UV-Vis Shimadzu UV-2500PC spectrophotometer according to the absorbance data of N-719 standard solutions.

The *J*–*V* curves of the sealed cells were measured under AM 1.5 illumination (100 mW cm⁻²) using a solar simulator (Yamashita Denso, YSS-80). The electrodes were illuminated from the substrate–electrode side. The incident photon to current conversion efficiency (IPCE) was measured by using a commercial setup (PV-25DYE, JASCO). The data from *J*–*V* curves and action

spectra represent the average behaviour for at least four cells of each sample.

The transient absorption (TAS) decays in the μs – ms timescale were measured on dye-sensitized electrodes. The setup has been described elsewhere.¹⁴ The study of the dye-sensitized films in a redox-inactive electrolyte (propylene carbonate) was carried out setting the excitation at 550 nm and monitoring the optical changes at a probe wavelength of 800 nm, whose amplitude is primarily dominated by dye cation absorption.¹⁵ Data were collected in the absence of an applied bias voltage under low-intensity excitation pulses corresponding approximately one injected electron per colloidal particle¹⁶ (average absorbance at the dye absorption maximum was 0.3). The TAS data for the pristine ZnO film were not possible to be measured because of its low transmittance.

Results and discussion

In the gallium-doped zinc oxide (ZnO:Ga), Ga³⁺ is expected to cause only a small lattice distortion because of their similar tetrahedral radii. Ga³⁺ ions also act as an efficient shallow donor in ZnO. However, gallium doping might give rise to spinel structures (M^{II}Ga₂O₄) when the matrix to be doped is ZnO, especially when heavily doped samples are taken into account.¹⁷ Solubility limits are reported to be close to 3 atom% of Ga in ZnO.^{18,19} The formation of ZnGa₂O₄ might take place in ZnO:Ga, changing the microscopic structural and electronic environment of Ga³⁺ in the ZnO matrix. In the normal cubic spinel crystal structure of ZnGa₂O₄, Zn²⁺ ions occupy tetrahedral sites and Ga³⁺ ions the octahedral ones. The powder X-ray diffraction (XRD) patterns of pure and gallium-modified zinc oxide (ZnO:Ga) nanoparticles are shown in Fig. 1. All samples have the zincite structure (JCPDS 14–3651) and there is no evidence of zinc gallate formation (ZnGa₂O₄), even in the ZnO:Ga 5 atom% nanoparticles.

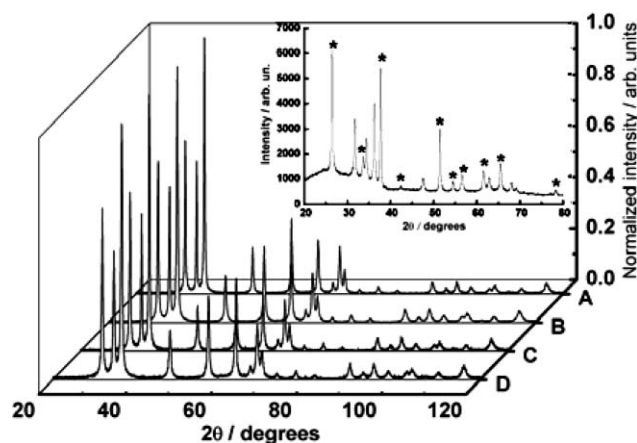


Fig. 1 Powder X-ray diffraction patterns of the nanoparticles synthesized by the precipitation method: (A) ZnO, (B) ZnO:Ga 1 atom%, (C) ZnO:Ga 3 atom% and (D) ZnO:Ga 5 atom%. Inset: X-ray diffraction pattern of the ZnO:Ga 5 atom% porous film. Asterisks denote FTO reflections.

The absence of ZnGa₂O₄ in the XRD patterns of ZnO:Ga nanoparticles is probably related to the low-temperature treatment employed: 150 °C for 2 h. The high crystallinity observed in the XRD patterns indicates the capability of preparing

nanocrystalline samples at low temperature by using the precipitation method.

The possibility of ZnGa_2O_4 formation in the porous film (after the heat treatment at 450°C for 30 min) was also evaluated by XRD. The XRD pattern of the $\text{ZnO}:\text{Ga}$ 5 atom% porous film deposited onto an FTO substrate is shown in Fig. 1 (see inset). Despite the FTO reflections it is possible to observe only the ZnO diffraction patterns, which indicates that ZnGa_2O_4 is not present in the gallium-modified zinc oxide porous electrodes even after the thermal treatment. The morphology of the films was analyzed by SEM (Fig. 2).

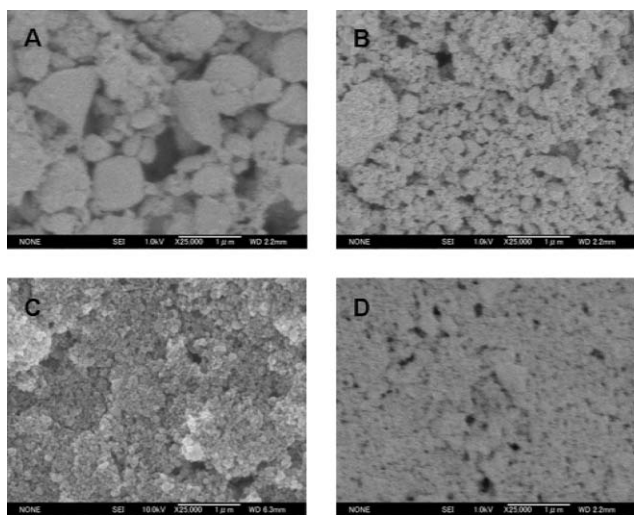


Fig. 2 FE-SEM images of the ZnO and $\text{ZnO}:\text{Ga}$ electrodes: (A) ZnO , (B) $\text{ZnO}:\text{Ga}$ 1 atom%, (C) $\text{ZnO}:\text{Ga}$ 3 atom% and (D) $\text{ZnO}:\text{Ga}$ 5 atom%.

The $\text{ZnO}:\text{Ga}$ films present smaller particle size than the ZnO electrode, as already observed for undoped TiO_2 compared to doped TiO_2 powders.⁴ This behavior was associated to an increased hydrolysis reaction rate for doped TiO_2 powders.⁴ A higher hydrolysis reaction rate is also believed to give rise to smaller particles of the gallium-modified samples in this work.

XPS data (Fig. 3) reveal a $\text{Ga } 2p_{3/2}$ peak located at 1119.0 eV, in good agreement with other reported values.^{20,21} This is an evidence that Ga ions exist as Ga^{3+} into the ZnO matrix. The intensity of the peak increases as the content of Ga^{3+} in the sample is also increased. Ga^{3+} ions are believed to be incorporated into the Zn^{2+} sites due to their radii similarity, leading to a substitutional doping. No shift in the $\text{O } 1s$ spectra (Fig. 3(b)) was observed, further evidencing the absence of a spurious phase related to Ga_2O_3 or even ZnGa_2O_4 .

The average pore size of the $\text{ZnO}:\text{Ga}$ electrodes was estimated from the BET method. The electrodes based on $\text{ZnO}:\text{Ga}$ 5 atom% present a relatively smaller and narrower pore size distribution than $\text{ZnO}:\text{Ga}$ 1 and 3 atom%. The average pore size of $\text{ZnO}:\text{Ga}$ 5 atom% electrodes was estimated to be 26 and ~ 60 nm for $\text{ZnO}:\text{Ga}$ 1 and 3 atom% electrodes, respectively. As observed in Table 1, the porosity increases with the increase in Ga^{3+} content. It is important to point out here that all samples, pristine and gallium-modified ZnO , were prepared using the same experimental procedure. Further improvements in the synthesis and deposition method are believed to enhance both porosity and adhesion of all samples to the TCO, respectively.

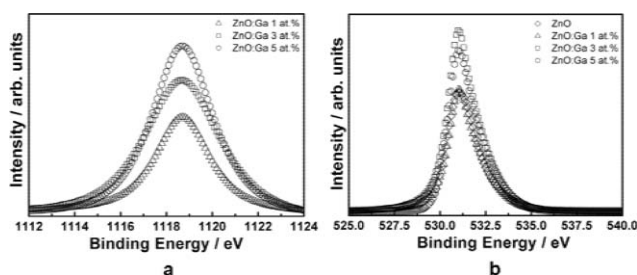


Fig. 3 Core level XPS spectra: (a) $\text{Ga } 2p$ and (b) $\text{O } 1s$ (Al- $\text{K}\alpha$ X-ray source).

The J - V curves of the DSSCs based on ZnO and $\text{ZnO}:\text{Ga}$ 1, 3 and 5 atom% under illumination of 100 mW cm^{-2} are shown in Fig. 4. Table 1 also summarizes the J - V characteristics of the sealed DSSCs and the amount of ruthenium dye absorbed for each electrode.

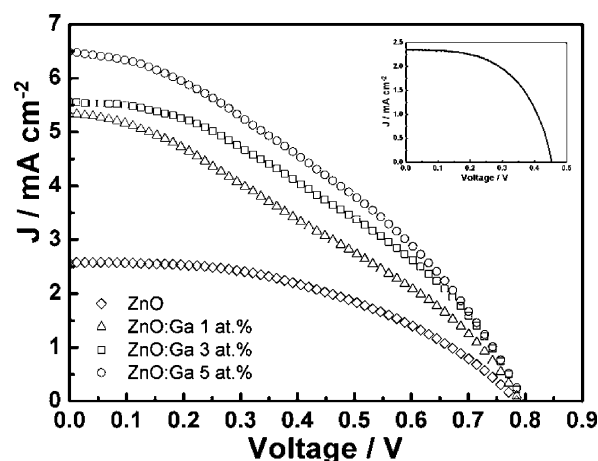


Fig. 4 J - V curves (AM 1.5, illumination intensity of 100 mW cm^{-2}) of the sealed DSSCs based on ZnO and $\text{ZnO}:\text{Ga}$ 1, 3 and 5 atom% films ($6 \mu\text{m}$) sensitized for 3 h in 0.5 mmol L^{-1} N-719 dye solution. Inset: J - V curve of a DSSC based on $\text{ZnO}:\text{Ga}$ 5 atom% with film thickness of $20 \mu\text{m}$ under 10 mW cm^{-2} .

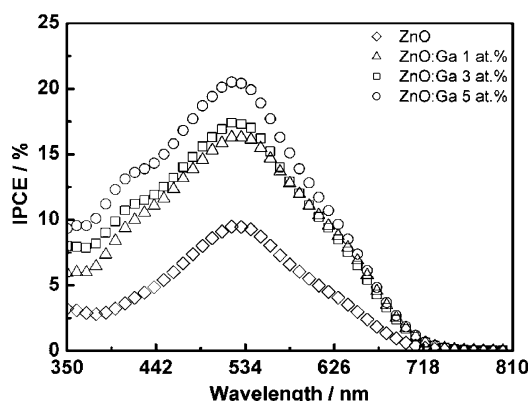
Values of open circuit voltage (V_{oc}) are close to 0.8 V, which are comparable to TiO_2 -based solar cells. Considering the film thickness employed ($6 \mu\text{m}$), the amount of ruthenium dye absorbed here is comparable to a $10 \mu\text{m}$ thick TiO_2 electrode ($\eta = 10\%$) sensitized by the N-3 dye²² ($1.3 \times 10^{-7} \text{ mol cm}^{-2}$) and also to a $20 \mu\text{m}$ thick $\text{ZnO}/\text{N-719}$ photoanode⁵ ($1.4 \times 10^{-7} \text{ mol cm}^{-2}$). The gallium modification resulted in more than a two-fold increase in photocurrent compared to the pristine ZnO . The DSSC based on $\text{ZnO}:\text{Ga}$ 5 atom% provided the highest photocurrent density indicating that gallium modification enables the preparation of electrodes with better electronic properties compared to non-intentionally modified ZnO . The higher photocurrent might, in part, be related to a large contribution to the density of states of ZnO arising from $\text{Ga } 3s$ states, especially due to their energetically highly delocalized nature near the Fermi level.²³ Conversion efficiencies (η) of 6% were achieved at a low light power density (10 mW cm^{-2}) for cells based on $\text{ZnO}:\text{Ga}$ 5 atom% with film thickness of $20 \mu\text{m}$ (Fig. 4, inset). This is one of the highest values reported so far for DSSCs based on ZnO systems under similar conditions. Kakiuchi *et al.* reported a η value of 4.6% under 14 mW

Table 1 Performance features from $J-V$ curves of DSSCs based on ZnO, ZnO:Ga 1, 3 and 5 atom% porous nanostructured electrodes under 100 mW cm^{-2} , along with porosity data and dye loading

DSSC	Porosity	$J_{sc}/\text{mA cm}^{-2}$	V_{oc}/V	FF	Dye loading/ mol cm^{-2}	Efficiency (%)
ZnO	0.16	2.07	0.79	0.46	—	0.74
ZnO:Ga 1 atom%	0.39	5.32	0.79	0.33	0.6×10^{-7}	1.4
ZnO:Ga 3 atom%	0.55	5.56	0.79	0.38	0.65×10^{-7}	1.7
ZnO:Ga 5 atom%	0.58	6.49	0.79	0.37	0.81×10^{-7}	1.9

cm^{-2} for a DSSC based on a $20 \mu\text{m}$ thick ZnO/N-719 photoanode.⁵ The low FF values reported here might be a consequence of the high series resistance losses arising from the poor adhesion between the ZnO:Ga nanoparticles and the TCO substrate.

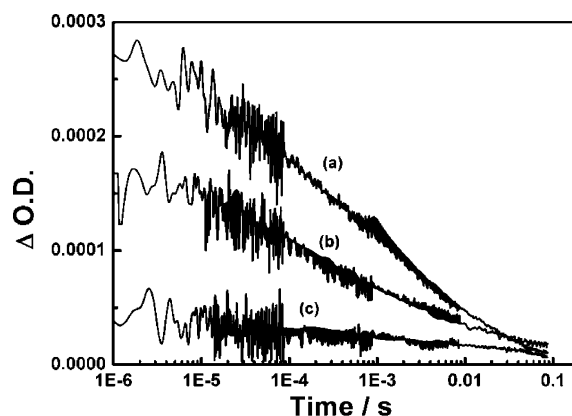
The IPCE curves of the DSSCs based on ZnO and ZnO:Ga resemble the absorption spectrum of the ruthenium dye (Fig. 5). An IPCE value of 20% was achieved by the DSSC based on ZnO:Ga 5 atom%.

**Fig. 5** IPCE curves (action spectra) of DSSCs based on ZnO and ZnO:Ga 1, 3 and 5 atom% as the nanostructured porous electrodes.

An improvement in the adhesion of the ZnO:Ga nanoparticles to the TCO substrate is expected to increase these efficiencies. An interesting difference in these action spectra and those usually reported for DSSCs based on TiO_2 is observed at long wavelengths. The low IPCE values around 700 nm, is an evidence of poor electron injection at long wavelengths due to the slightly higher conduction band edge of ZnO compared to TiO_2 . This effect will be discussed in further detail in a future publication.

To address the effect of the gallium modification on the zinc dissolution and to analyse how this can affect the amount of ruthenium dye absorbed, and as a consequence, the formation of dye aggregates, two equal volumes of buffer solution (Synth, pH 4) were added to two vessels at room temperature. A non-sensitized ZnO porous film at temperature around $80 \text{ }^\circ\text{C}$ was immersed into the buffer solution and the same procedure was done simultaneously using a ZnO:Ga 5 atom% porous film. The immersion time was 3 h (equal to the sensitization time used in this work). After this period both ZnO and ZnO:Ga 5 atom% films were completely dissolved. Therefore, gallium doping does not affect the solubility of ZnO films.

Fig. 6 shows the charge recombination decays from μs to ms for the ZnO:Ga films using a redox inactive electrolyte. Transient data were collected at 800 nm, monitoring the induced absorption of dye cations generated by electron injection into the ZnO:Ga films.

**Fig. 6** Transient absorption spectra of ZnO:Ga porous films sensitized by the N-719 dye: (a) ZnO:Ga 5 atom%, (b) ZnO:Ga 3 atom% and (c) ZnO:Ga 1 atom%. The probe wavelength was 800 nm, where the signal is mainly due to the dye radical cation absorption. The excitation wavelength was 550 nm.

The characteristic non-exponential kinetics reported for TiO_2 and ZnO electrodes²⁴ is also observed here, indicating that the recombination dynamics are controlled by electron transport through an energetic distribution of trap states within the metal oxide film.²⁵ The recombination half time values, $t_{50\%}$, observed in this work are $\sim 300 \mu\text{s}$, a little faster than typical values reported for TiO_2 electrodes²⁵ ($800 \mu\text{s}$) but slower than those measured for SnO_2 ($4 \mu\text{s}$).²⁵

The increase in the amplitude of the transient absorption signal with gallium level is striking, indicating an order of magnitude increase in the yield of dye cations with increased Ga density. This increase in amplitude appears to be significantly larger than the increase in the amount of ruthenium dye absorbed, and therefore can not be attributed primarily to an increase in light absorption. Rather, the observed increase in the dye cation yield suggests more efficient electron injection from the dye excited state. Such more efficient electron injection most plausibly stems from faster electron injection kinetics due to an increase of the number of acceptor states in the semiconductor. This increased electron injection yield correlates well with the increase in photocurrent density.

Conclusions

The gallium modification in ZnO produced a smaller particle size, higher porosity and surface area. No evidence of ZnGa_2O_4 or any other contaminant phase was observed even in the ZnO:Ga 5 atom% porous film. As evidenced from the characteristic binding energies, Ga is present in the ZnO matrix as Ga^{3+} . The increase in dye cation yield observed by TAS indicated a more efficient

electron injection from the dye excited state, possibly associated with a faster electron injection kinetics. High performance DSSCs may be assembled based on ZnO:Ga porous nanostructured electrodes with a η value as high as 6% at low light intensity.

Acknowledgements

We thank Fapesp, CNPq and Renami for the financial support. A. S. G. and J. N. F. thank Fapesp for the scholarships. A. S. G. thanks Capes for the scholarship and Brian O'Regan for helpful discussions. The authors also thank C. O. Paiva-Santos and S. G. Antônio for the XRD measurements.

References

- 1 B. O'Regan and M. Gratzel, *Nature*, 1991, **353**, 737–740.
- 2 J. M. Kroon, N. J. Bakker, H. J. P. Smit, P. Liska, K. R. Thampi, P. Wang, S. M. Zakeeruddin, M. Gratzel, A. Hinsch, S. Hore, U. Wurfel, R. Sastrawan, J. R. Durrant, E. Palomares, H. Pettersson, T. Gruszecki, J. Walter, K. Skupien and G. E. Tulloch, *Prog. Photovoltaics*, 2007, **15**, 1–18.
- 3 T. Ma, M. Akiyama, E. Abe and I. Imai, *Nano Lett.*, 2005, **5**, 2543–2547.
- 4 K. H. Ko, Y. C. Lee and Y. J. Jung, *J. Colloid Interface Sci.*, 2005, **283**, 482–487.
- 5 K. Kakiuchi, E. Hosono and S. Fujihara, *J. Photochem. Photobiol., A*, 2006, **179**, 81–86.
- 6 K. Keis, E. Magnusson, H. Lindstrom, S.-E. Lindquist and A. Hagfeldt, *Sol. Energy Mater. Sol. Cells*, 2002, **73**, 51–58.
- 7 H. Horiuchi, R. Katoh, K. Hara, M. Yanagida, S. Murata, H. Arakawa and M. Tachiya, *J. Phys. Chem. B*, 2003, **107**, 2570–2574.
- 8 R. Katoh, A. Furube, Y. Tamaki, T. Yoshihara, M. Murai, K. Hara, S. Murata, H. Arakawa and M. Tachiya, *J. Photochem. Photobiol., A*, 2004, **166**, 69–74.
- 9 K. Keis, L. Vayssieres, H. Rensmo, S.-E. Lindquist and A. Hagfeldt, *J. Electrochem. Soc.*, 2001, **148**, A149–A155.
- 10 H. Rensmo, K. Keis, H. Lindstrom, S. Sodergren, A. Solbrand, A. Hagfeldt, S. E. Lindquist, L. N. Wang and M. Muhammed, *J. Phys. Chem. B*, 1997, **101**, 2598–2601.
- 11 T. Minami, H. Sato, H. Nanto and S. Takata, *Jpn. J. Appl. Phys.*, 1985, **24**, L781–L784.
- 12 S.-M. Park, T. Ikegami and K. Ebihara, *Thin Solid Films*, 2006, **513**, 90–94.
- 13 M. Nonaka, S. Matsushima, M. Mizuno and K. Kobayashi, *Chem. Lett.*, 2002, 580–581.
- 14 H. Ohkita, S. Cook, T. A. Ford, N. C. Greenham and J. R. Durrant, *J. Photochem. Photobiol., A*, 2006, **182**, 225–230.
- 15 S. A. Haque, Y. Tachibana, R. L. Willis, J. E. Moser, M. Gratzel, D. R. Klug and J. R. Durrant, *J. Phys. Chem. B*, 2000, **104**, 538–547.
- 16 S. A. Haque, Y. Tachibana, D. R. Klug and J. R. Durrant, *J. Phys. Chem. B*, 1998, **102**, 1745–1749.
- 17 A. S. Gonçalves, S. A. M. Lima, M. R. Davolos, S. G. Antônio and C. O. Paiva-Santos, *J. Solid State Chem.*, 2006, **179**, 1330–1334.
- 18 N. Roberts, R. P. Wang, A. W. Sleight and W. W. Warren, *Phys. Rev. B*, 1998, **57**, 5734.
- 19 R. Wang, A. W. Sleight and D. Cleary, *Chem. Mater.*, 1996, **8**, 433–439.
- 20 M. Passlack, E. F. Schubert, W. S. Hobson, M. Hong, N. Moriya, S. N. G. Chu, K. Konstadinidis, J. P. Mannaerts, M. L. Schnoes and G. J. Zyzik, *J. Appl. Phys.*, 1995, **77**, 686–693.
- 21 V. Bhosle, A. Tiwari and J. Narayan, *J. Appl. Phys.*, 2006, **100**, 033713–033716.
- 22 M. K. Nazeeruddin, A. Kay, I. Rodicio, R. Humphrybaker, E. Muller, P. Liska, N. Vlachopoulos and M. Gratzel, *J. Am. Chem. Soc.*, 1993, **115**, 6382–6390.
- 23 Y. Imai and A. Watanabe, *J. Mater. Sci.*, 2005, **15**, 743–749.
- 24 R. L. Willis, C. Olson, B. O'Regan, T. Lutz, J. Nelson and J. R. Durrant, *J. Phys. Chem. B*, 2002, **106**, 7605–7613.
- 25 A. N. M. Green, E. Palomares, S. A. Haque, J. M. Kroon and J. R. Durrant, *J. Phys. Chem. B*, 2005, **109**, 12525–12533.